Resilient Cities and Structures 2 (2023) 103–119

Contents lists available at ScienceDirect

Resilient Cities and Structures

journal homepage: www.elsevier.com/locate/rcns

Full Length Article

Seismic collapse assessment of archetype frames with ductile concrete beam hinges

Hasan Tariq[a], Ezra A. Jampole[b], Matthew J. Bandelt[c,*]

[a] Thornton Tomasetti, New York, NY, USA
[b] Buildings and Structures Group, Exponent, New York, NY, USA
[c] John A. Reif, Jr., Dept. of Civil and Environmental Engineering, New Jersey Institute of Technology, Newark, NJ, USA

ARTICLE INFO

Keywords:
Lumped-plasticity model
Archetype frames
HPFRCC Plastic-hinge
Collapse assessment
Mean annual frequency of collapse

ABSTRACT

Highly ductile cement-based materials have emerged as alternatives to conventional concrete materials to improve the seismic resistance of reinforced concrete (RC) structures. While experimental and numerical research on the behavior of individual components has provided significant knowledge on element-level response, relatively little is known about how ductile cement-based materials influence system-level behavior in seismic applications. This study uses recently developed lumped-plasticity models to simulate the unique failure characteristics and ductility of reinforced ductile-cement-based materials in beam hinges and applies them in the assessment of archetype frame structures. Numerous story heights (four, eight, and twelve), frame configurations (perimeter vs. space), materials (conventional vs. ductile concrete), and replacement mechanisms within the beam hinges are considered in the seismic analysis of the archetype structures. Results and comparisons are made in terms of the probability of collapse at 2% in 50-year ground motion, mean annual frequency of collapse, and adjusted collapse margin ratio (ACMR) across archetype structures. The results show that engineered HPFRCCs in beam plastic-hinge regions can improve the seismic safety of moment frame buildings with higher collapse margin ratios, lower probability of collapse, and the ability to withstand large deformations. Data is also reported on how ductile concrete materials can reduce concrete volume and longitudinal reinforcement tonnage across frame configurations and story heights while maintaining or improving seismic resistance of the structural system. Results demonstrate future research needs to assess life-cycle costs, predict column hinge behavior, and develop code-based design methods for structural systems using highly ductile concrete materials.

1. Introduction

Reinforced concrete (RC) members are designed to resist lateral forces and are detailed to undergo large inelastic flexural deformations in plastic hinge regions [1,2]. In seismic lateral resisting systems, beams are typically designed with lower strengths compared to columns to ensure damage occurs in beams rather than columns to reduce the likelihood of forming a story mechanism which is essential for structural stability [2]. Problems related to reinforcement congestion and concrete consolidation issues are often encountered when trying to achieve the desired detailing in plastic-hinge regions [3,4]. High-performance fiber-reinforced cementitious composites (HPFRCCs) [5,6] have emerged as a potential solution where applications in structural components have shown significantly enhanced load carrying capacity [7,8], ductility [9,10], and damage tolerance [11–13] while minimizing transverse reinforcement requirements and reducing congestion.

Unlike traditional reinforced concrete flexural members without axial loads which predominantly fail due to crushing, reinforced HPFRCC flexural members without axial loads often fail due to tensile rupture of the mild rebar [14,15]. While failure generally occurs at high levels of deformation, certain HPFRCC material properties or reinforcement ratios can cause failure at low levels of deformation when a tensile crack localizes, causing a loss in strength that cannot be compensated by the post-crack localization contribution of the reinforcing steel [16]. These changes in behavior necessitate a review of how various material properties and structural characteristics influence component- and system-level response.

Recent numerical studies have built on experimental research to predict deformation capacity [17], understand factors that influence structural response in greater detail [16,18], and predict plastic-hinge response [19–21]. In a recent study by the authors [22], a spring-hinge modeling approach was developed to simulate the response of reinforced HPFRCC beams under cyclic loading. The model was further applied to investigate the seismic performance of a four-story archetype reinforced concrete frame with HPFRCC beams. Results showed an increase in the collapse margin ratio and a reduction in the probability

* Corresponding author.
E-mail addresses: htariq@thorntontomasetti.com (H. Tariq), ejampole@exponent.com (E.A. Jampole), bandelt@njit.edu (M.J. Bandelt).

https://doi.org/10.1016/j.rcns.2023.02.008
Received 22 December 2022; Received in revised form 24 February 2023; Accepted 26 February 2023
Available online 5 March 2023

of collapse when comparing a tailored HPFRCC frame to a traditional RC frame model.

This paper builds on the authors' recent work by assessing the performance of a group of buildings containing HPFRCC beams in the lateral resisting system. The buildings are selected from a suite of structures analyzed and designed by Haselton et al. [23]. Due to the limited availability of plastic hinge modeling of axially loaded members [22,24–26], columns are not considered within the scope of this study. The buildings include variations in frame types and number of stories. The assessment considers design alternatives that can be utilized to improve the performance of RC frames by incorporating ductile concrete materials. The results show the probabilistic performance of RC frames using HPFRCC materials, and the implications of material replacement on seismic performance are discussed.

2. Design principle for reinforced HPFRCC frames

Moment-resisting frames are designed against the target base shear by incorporating the response modification factor (R), which illustrates the degree of expected inelastic deformation and ductility capacity. The framing elements are sized and reinforcement is detailed to resist the internal actions from flexure, shear, and axial effects due to the lateral sway of the building from seismic excitations. The sizing and reinforcement detailing requirements of moment-resisting frame buildings are intended to ensure uniform distribution of damage along the height of the building by achieving strong-column/weak-beam design, thereby preventing brittle shear failures and enabling the flexural yielding in the plastic-hinge regions [2,27–29]. The strong-column/weak-beam principle is of paramount importance in achieving the safety of buildings under earthquakes. This allows for uniform distribution of lateral drift and helps avoid a soft-story phenomenon. This study focused on replacing RC beam hinges with reinforced HPFRCC hinges because the modeling approach was calibrated to an experimental database limited to beams due to limited experimental data for reinforced HPFRCC columns [22]. Hence, possible design approaches for reinforced HPFRCC beam sections are discussed.

Moment-resisting frame buildings are usually designed for target base-shear strengths, which are less than the strength required to keep the structure elastic based on the response spectra [30]. Thus, the building will experience an inelastic response under ground shaking. Previous experimental testing and numerical studies have suggested certain design principles for RC members to ensure a ductile response without premature degradation in strength. These principles include: maintaining strong column-weak beam ratios, detailing for the plastic hinge regions, and avoiding brittle failures (shear and axial) [2,27–29]. Among all, the strong column-weak beam ratio is of paramount importance for the distribution of damage along the height of the building. If a building has weak columns, the damage will concentrate on one or a small number of stories leading to structural collapse. On the other hand, if the columns are stronger than beams by a sufficient margin, then damage will be more uniform, provided that plastic-hinge regions satisfy ductility requirements. It is worth noting that columns in a particular story support the weight of the building above, whereas beams resist the tributary gravity loads only. Therefore, the failure of a column can quickly lead to a complete collapse of a building. This study focused on replacing RC beam hinges with reinforced HPFRCC hinges because the modeling approach was calibrated to an experimental database limited to beams due to a lack of experimental data for reinforced HPFRCC columns [22]. Hence, possible design approaches for reinforced HPFRCC beam sections are discussed.

The bending moment at yield for an RC beam hinge was calculated based upon the Whitney stress block assumption [23] as shown in Fig. 1e. The yield strength for reinforced HPFRCC members was based upon stress and strain distribution considered by Tariq et al. [22] and Pokhrel and Bandelt [19] (Fig. 1f). Since the ultimate tensile strain of HPFRCC exceeds the yield strain of the steel observed during tension stiffening experiments [31], the yield moment capacity considered the tensile strength of HPFRCC in tension along with yield strength of steel [22]. Initial analysis showed higher moment capacity of reinforced HPFRCC beams as compared to the RC beam under the same cross-section (b, h) and reinforcement details (ρ^t, ρ^b), as expected. The increase in the moment strength ranged between 10% and 95% with

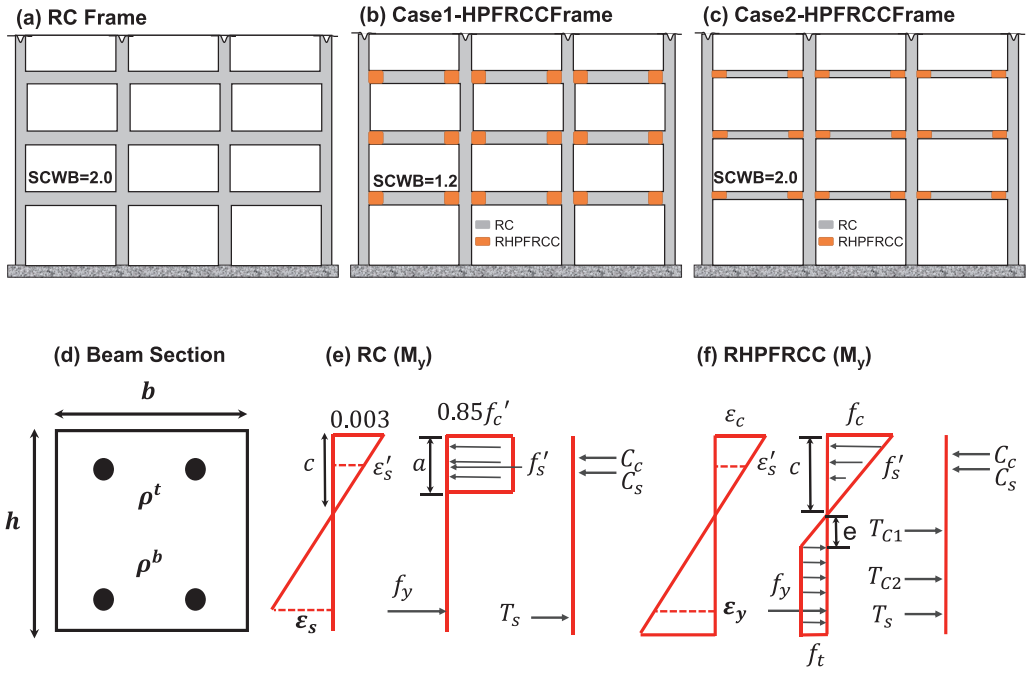

Fig. 1. (a) RC Frame (b) Case1-HPFRCC frame (c) Case2-HPFRCC frame (d) Beam section (e) Stress strain profile for RC section (f) stress strain profile for reinforced HPFRCC section.

an average of 38% which led to a reduction in the strong column-weak beam (SCWB) ratio at each joint, with an average reduction of 37.5% as compared to SCWB in conventional RC frames [23].

Based upon this rationale, two HPFRCC frame configurations were considered in this study, and the results were compared with a traditional RC frame model (Fig. 1a-c). In the first model, the HPFRCC beam hinge properties were based on the RC beam sections designed by Haselton et al. [23] and are referred to herein as the "Case1-HPFRCC" frame. This frame can be thought of as a simple material replacement of concrete for HPFRCC in beam hinge regions without any consideration to changes in structural components or system response. In the second frame model, the section height (h) and reinforcement details (ρ^t, ρ^b) were designed to ensure the same value of SCWB ratio as the RC frame model named as the "Case2-HPFRCC" frame.

The flexural behavior of reinforced HPFRCC beams was considered where the deformation capacity increases by increasing the reinforcement ratio [32]. The effect of reinforced HPFRCC beams on joint shear capacity and slab punching failure was not considered. An iterative process was adopted for the design of reinforced HPFRCC beams. The first step was to solve for beam height (h) under the same reinforcement ratio (ρ^t, ρ^b) against the target moment of an RC cross-section at the yield level based on Equation 1 from Tariq et al. [22]

The depth of the reinforced HPFRCC beam was incrementally decreased until the yield strength approached the desired strength. Then the reinforcement ratio was adjusted to match the strength of the RC beams. The cross-section details including element size (b, h) and longitudinal reinforcement ratio (ρ^t, ρ^b) of Case2-HPFRCC beams for all considered frames are archived in Appendix A. Column sizes were all the same for RC, Case1-HPFRCC, and Case2-HPFRCC frames. The beams are 46cm × 46cm to 76cm × 81cm and have the positive and negative reinforcement ratios of 0.35% to 1.2% and 0.5% to 2.0%, respectively.

3. Collapse assessment methodology

A seismic collapse risk assessment was performed by utilizing a performance-based earthquake engineering (PBEE) approach, which correlates the site-specific ground shaking with the expected response through nonlinear time history analysis to predict the probabilistic damage or collapse (Fig. 2). This method has been used by numerous researchers to predict the probabilistic seismic performance of various reinforced concrete and steel structures [23,33,34]. In this research, the process began by identifying archetype buildings with variations in building heights, bay widths, and frame configurations. The next step was to idealize the archetype models to reflect the response of the structural system. A minimum number of bays were identified to account for an overturning moment on the exterior and interior frames. The modeling parameters of various components of the archetype structures were calculated based on expected material properties and the models have the ability to capture cyclic strength degradation under large cyclic reversals (Fig. 2a).

The collapse performance was evaluated through incremental dynamic analysis (IDA) under a prescribed set of ground motions; each scaled linearly to higher intensity levels until one or several stories of the model became dynamically unstable, referred to herein as side-sway collapse. The nonlinear analysis must fully converge at large deformations to predict collapse. A variety of nonlinear solutions algorithms were used to satisfy the dynamic equation of equilibrium at each time step, such as a Newton Solution, Modified Newton Solution, and Krylov Newton Solution. If the selected algorithm was unable to satisfy the system of equations within specified tolerances, different solutions algorithms were attempted automatically. [35]

The structural response was quantified in terms of the maximum story drift ratio adopted as an engineering demand parameter. The 5% damped spectral acceleration, $Sa(T_1)$, corresponding to the fundamental period (T_1) was then correlated with maximum story drift ratio in the form IDA curves (Fig. 2b). IDA curves were reported for the controlling component of each record pair to account for the three-dimensional effect of the building. The median IDA curve was then computed for each archetype model, and the uncertainty associated with record-to-record variability ($\sigma_{ln,RTR}$) was then reported. The spectral accelerations at collapse were further processed through statistical means to compute fragility curves to better understand the variability in the response [36]. The collapse capacity was adjusted to account for variability in the spectral shape (ε), and modeling ($\sigma_{ln,modeling} = 0.5$) uncertainty based on guidelines proposed by Haselton et al. [37] (Fig. 2c).

The final step was to calculate the mean annual frequency of collapse (λ_{col}), which required integrating the site-specific hazard curve (Fig. 2d), which gives the probability of exceeding a ground motion intensity, and the model's adjusted collapse fragility curve, which informs the collapse probability of a structure corresponding to particular intensity measure, $Sa(T_1)$. The mean annual frequency of collapse (λ_{col}) was also calculated. This metric is used to predict seismic performance and describes how likely a structure is going to collapse given the structure's collapse capacity and site-specific seismic hazard.

4. Description of archetype buildings

Six buildings were selected from the suite of buildings analyzed and designed by Haselton et al. [23] and are summarized in Table 1. These buildings were representative of low to medium-rise office buildings located in Northern California, Los Angeles [23]. The corresponding coordinates of the site are 33.996° Lat., −118.16° Long. and classified as Site Class D based on soil properties. The buildings range from four to twelve stories and further comprise of two different configurations: perimeter and space frame buildings. Fig. 3a-b shows the layout of building configurations where the frames were designed to resist gravity and lateral loads for space frame buildings, and exterior frames resisted lateral loads for the perimeter frame buildings.

The height of the bottom story was 4.57 m, while the upper stories were 3.96 m high for all the buildings Fig. 3c-e. The columns were uniformly spaced at 9.1 m for four-story buildings and 6.1 m for eight and twelve-story buildings. The design of each archetype was based on code-based prescriptive procedures following ACI 318 [38] and ASCE7 [39]. Further details on structural design can be found in Haselton et al. [23].

Member sizes were governed by strength requirements, strong column weak beam provisions, joint shear requirement and allowable story drifts under design seismic forces. The beam cross-sections were uniform in perimeter frame buildings, and section sizes were stepped down for space frame buildings. The column cross-sections were the same for exterior and interior bays in space frame buildings. The interior columns were larger as compared to exterior columns in perimeter frame buildings. The geometric details of structural sections can be found in Appendix A.

Table 1
Design Information for Modern RC Special Moment Resisting Frame Buildings [23].

Frame ID [#]	Frame Configuration -	Stories [#]	Bay Width [m]	Foundation Fixity -
1009	Perimeter	4	9.1	GB
1010	Space	4	9.1	GB
1011	Perimeter	8	6.1	GB
1012	Space	8	6.1	GB
1013	Perimeter	12	6.1	GB
1014	Space	12	6.1	GB

A- Strength and Stifness stepped as per common design practice
GB- "Grade Beam"-includes rotational stiffness of grade beam

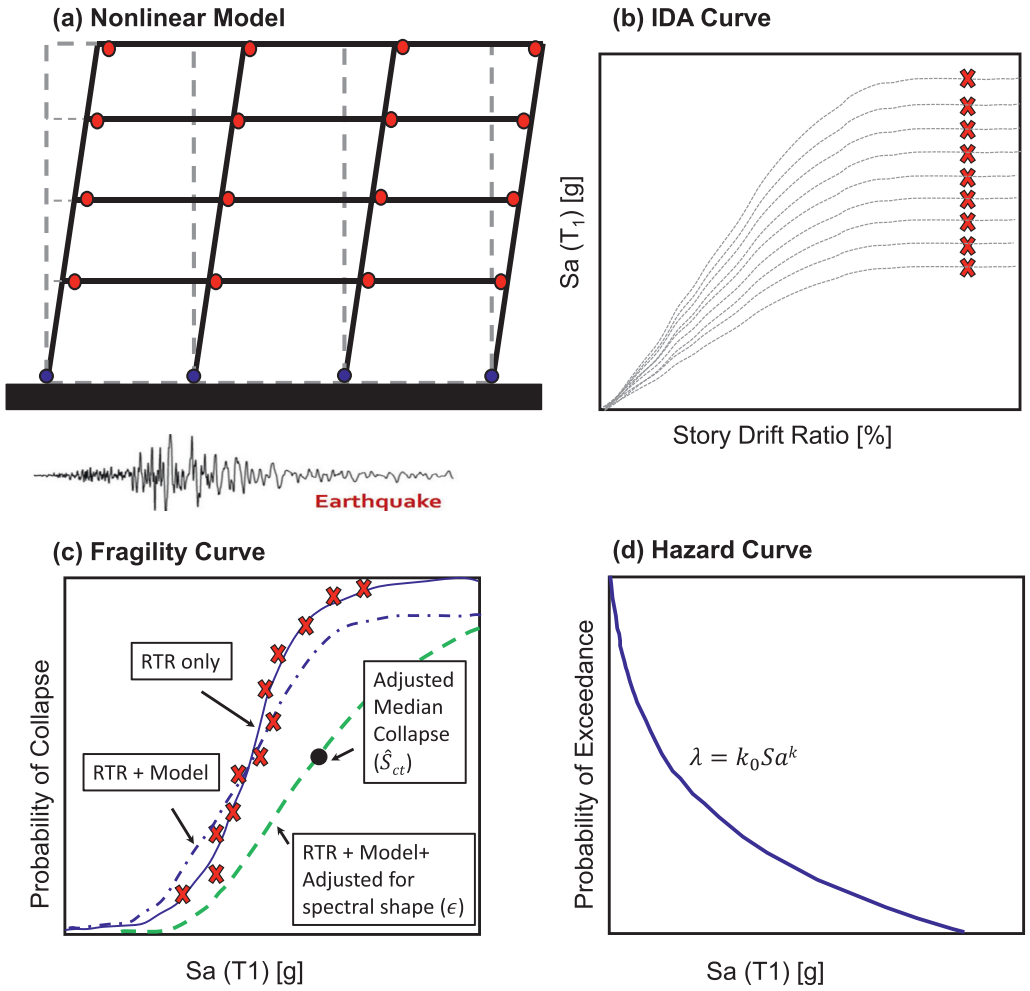

Fig. 2. Concept of probabilistic collapse assessment.

5. Modeling of archetype frames

In this study, a two-dimensional three-bay model was employed for the purpose of collapse risk investigation as identified in Fig. 3a-b for both the space and perimeter frame buildings. The selection of three bays was governed by the model's ability to account for the behavior of exterior and interior frames. The analysis of the models was performed in OpenSees, an open-source platform for earthquake engineering simulations [40]. The schematic representation of the analysis model along with key aspects are shown in Fig. 4. The structural components were modeled by elastic beam-column elements with nonlinear behavior confined to the end regions and represented by rotational springs.

The reliable prediction of seismic performance relies on the ability of the model to capture the material and section deterioration in the form of cyclic degradations at large deformations. To this end, the nonlinear behavior of RC hinges was modeled by the Ibarra-Medina Krawinkler (IMK) model with a peak-oriented hysteretic response as shown in Fig. 3c [41]. The hysteretic properties of the model, such as initial stiffness (k_e), yield moment (M_y), Maximum to yield moment ratio (M_u/M_y), plastic rotation (θ_p), post capping rotation (θ_{pc}), residual strength ratio (M_r/M_y) and cyclic strength degradation parameter (λ) were obtained from the empirical equations developed by Haselton et al. [23].

The inelastic behavior of reinforced HPFRCC beam hinges was represented by the Pinching4 hysteretic model [42] as illustrated in Fig. 3d. Key parameters of the model include; yield moment (M_y), ultimate moment (M_u), capping moment (M_c), residual moment (M_r), yield rotation (θ_y), ultimate rotation (θ_u), capping rotation (θ_c), residual rotation (θ_r) and energy based cyclic strength degradation parameter (f_2). The modeling properties were based on the approaches and empirical equations developed by Tariq et al. [22].

The effect of cracking at the column footing joint was incorporated by modeling a semi-rigid rotational spring at the base of the first story column (Fig. 4a). The elastic stiffness of the footing spring was based on the grade beam and soil stiffness. The flexibility at the beam-column joint due to shear cracking was also considered by modeling a finite length two-dimensional joint represented by the 'Joint2D' model [43]. All modeling parameters were based on the actual material properties. The compressive strength of the concrete was 35 MPa. The material properties of HPFRCC comprised compressive strength, 35 MPa; tensile strength, 2.2 MPa; and modulus of elasticity, 25,000 MPa. Values were chosen to simulate a mixture for large-scale mix design [44]. Further, the yield and ultimate strength of the reinforcing bars were 462 MPa and 690 MPa. The mechanical properties of concrete, HPFRCC, and reinforcing materials are also summarized in Table 2. Other details, such as rotational stiffness of footing and joint spring, transverse reinforcement ratio, and spacing, can be found in Haselton et al. [23].

The expected gravity loads were calculated based on the tributary area, including 1.05 times the dead load (8.4 kN/m^2) and 0.25 times the live load (2.4 kN/m^2) [45]. The loads were applied to the beam in the form of uniformly distributed load (W_{trib}). Similarly, a uniform mass was assigned to each joint, and tributary widths were used in calculating

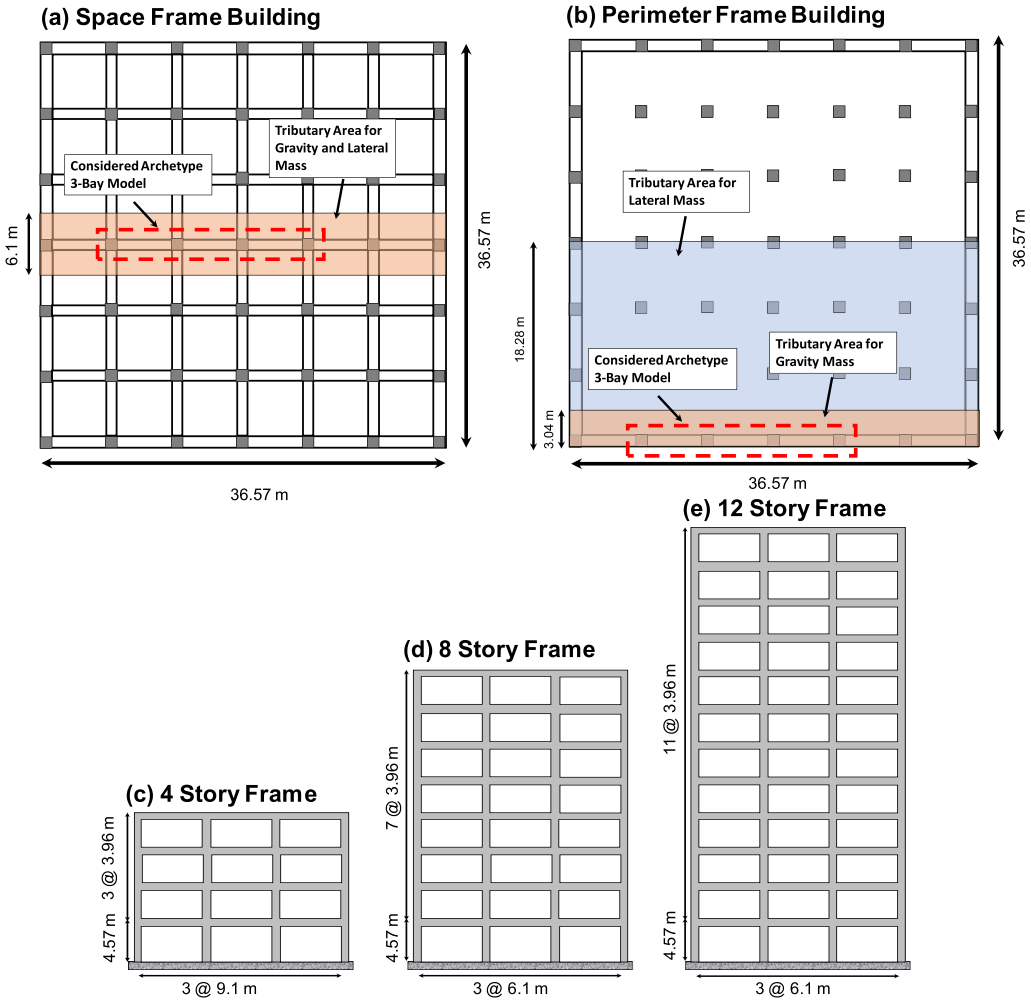

Fig. 3. Layout of considered archetypical buildings plan and elevation (a) space frame building plan (b) perimeter frame building plan (c) four-story (d) eight-story (e) twelve-story.

Table 2
Pertinent mechanical properties.

Description	Units	HPFRCC Frame	RC Frame
Modulus of Elasticity	MPa	25,000	27,800
Compressive Strength	MPa	35	35
Tensile Strength	MPa	2.2	-
Rebar Yield Strength	MPa	462	462
Rebar Ultimate Strength	MPa	490	-
Gravity Loads	KN/m^2	8.4	8.4

the seismic mass equal to the bay width for the space frame and half of the total width of the building for the perimeter frame as shown in Fig. 3a-b. For the case of the perimeter frame structures, the gravity loads that were not part of the primary lateral load resisting system were also considered to account for additional P-delta forces that the gravity system imposes on the perimeter frame by modeling a fictitious "leaning column". The loads (W_{axial}) corresponding to each floor were assigned to leaning (P-△) columns which were connected to the primary frame with axially rigid struts.

Composite action from the beam and slab was also considered in terms of calculating the strength following the approach developed by ACI [2] and stiffness based on the recommendations provided by Robertson [46]. Moreover, Rayleigh damping corresponding to 5% critical damping was applied to the first and third modes following the guidelines proposed by Zareian and Medina [47].

The fundamental period (T_1) of all archetype frame models calculated from eigenvalue analysis are reported and compared in Table 3 and Fig. 5. The results for RC, Case1-HPFRCC, and Case2-HPFRCC frame models are represented by black, red, and green lines and further distinguished by bar types for space (solid) and perimeter (hatched) frames. It was observed that the natural period increased with height of the building, as shown in Fig. 5. As expected, the reported periods for reinforced HPFRCC frame models were greater than RC frame models due to the lower modulus of elasticity (E). Moreover, the natural period for Case2-HPFRCC frame models was greater than RC and Case1-HPFRCC frame models by 15% and 12%, on average, due to the smaller section depth (h) and modulus of elasticity (E).

6. Seismic hazard

A set of 40 pairs of earthquake records, each with two orthogonal horizontal components, were chosen for incremental dynamic analysis in this study. The details regarding the acceleration time history of the ground motion records were obtained from Haselton et al. [23] where these records were also used for the collapse assessment of modern reinforced concrete buildings. The selection and scaling of the ground motion was conducted by Goulet et al. [48] where the 80 ground motions

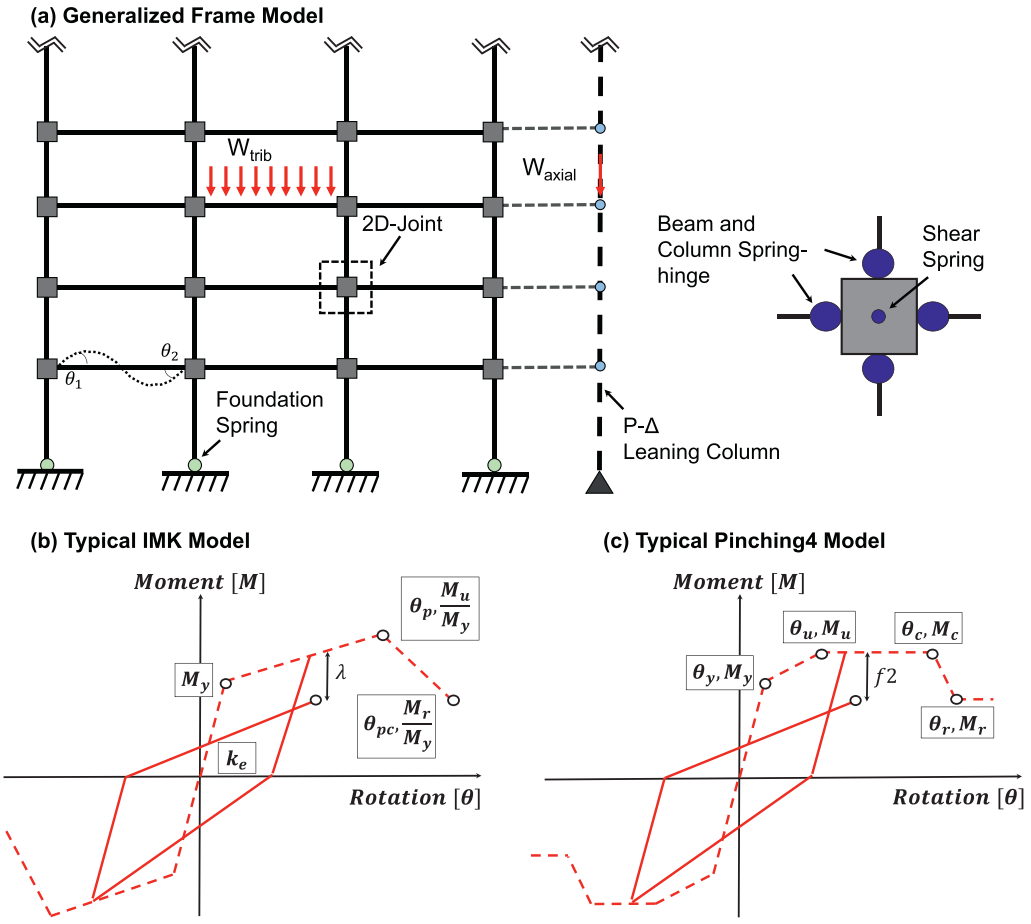

Fig. 4. (a) Schematic representation of analysis model for archetype frame (b) typical IMK model for RC beam and column hinges (c) typical Pinching4 model for HPFRCC beam hinges.

Table 3
Summary of Collapse Risk Assessment Results for Archetype Frames.

Design ID	Stories	Frame Type	Model Type	Period [sec]	$\hat{S}_{ct}$ [g]	ACMR [-]	P[2/50] [-]	$\sigma_{ln,total}$ [-]	$\lambda_{col} \times 10^{-4}$ [col/year]
1009	4	Perimeter	RC-Haselton	1.16	1.87	2.51	0.08	0.65	2.10
			RC-model	1.17	1.82	2.49	0.09	0.67	2.79
			Case1-HPFRCC	1.21	1.44	2.02	0.14	0.66	4.51
			Case2-HPFRCC	1.38	1.76	2.71	0.06	0.66	2.09
1010	4	Space	RC-Haselton	0.86	3.17	3.40	0.03	0.65	0.70
			RC-model	0.86	3.13	3.36	0.03	0.68	1.14
			Case1-HPFRCC	0.91	2.54	2.90	0.05	0.64	1.58
			Case2-HPFRCC	1.04	2.79	3.52	0.02	0.62	0.87
1011	8	Perimeter	RC-Haselton	1.71	1.00	1.77	0.19	0.64	6.30
			RC-model	1.72	0.93	1.71	0.21	0.65	6.80
			Case1-HPFRCC	1.75	0.87	1.62	0.23	0.65	7.56
			Case2-HPFRCC	1.97	1.00	2.11	0.12	0.65	3.96
1012	8	Space	RC-Haselton	1.8	1.23	2.29	0.09	0.62	2.40
			RC-model	1.8	1.21	2.31	0.10	0.65	3.13
			Case1-HPFRCC	1.84	1.10	2.17	0.12	0.65	3.78
			Case2-HPFRCC	1.98	1.17	2.47	0.08	0.65	2.78
1013	12	Perimeter	RC-Haselton	2.01	0.85	1.84	0.16	0.62	5.20
			RC-model	2.02	0.83	1.78	0.18	0.63	5.55
			Case1-HPFRCC	2.06	0.74	1.61	0.25	0.71	11.50
			Case2-HPFRCC	2.4	0.82	2.02	0.14	0.65	7.11
1014	12	Space	RC-Haselton	2.14	0.83	1.91	0.15	0.62	4.70
			RC-model	2.19	0.82	1.86	0.16	0.63	5.43
			Case1-HPFRCC	2.23	0.60	1.38	0.29	0.59	12.00
			Case2-HPFRCC	2.48	0.79	1.98	0.13	0.60	6.61

$\hat{S}_{ct}$: Adjusted median collapse; ACMR : Adjusted collapse margin ratio; P[2/50]= Probability of collapse at 2% in 50 years motion
$\sigma_{ln,Total} = \sqrt{\sigma^2_{ln,RTR} + \sigma^2_{ln,modeling}}$; λ_{col} : Mean annual frequency of collapse

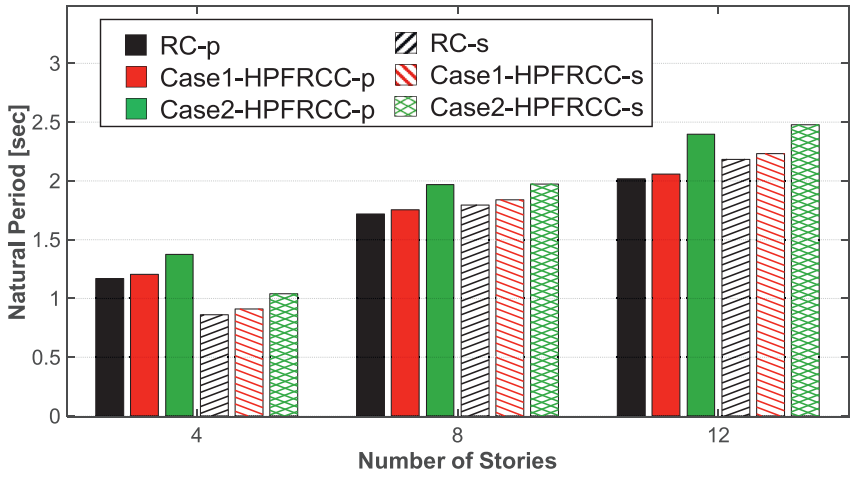

Fig. 5. Effect of number of stories on natural period.

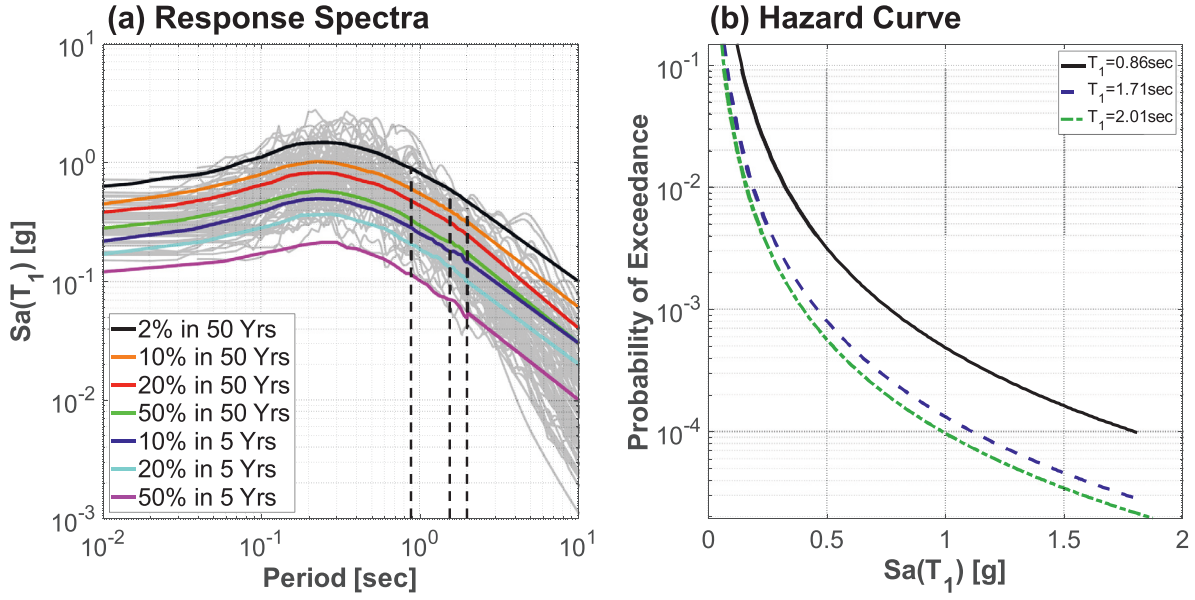

Fig. 6. (a) Response spectra of individual ground motions and spectra for various levels of intensity (b) Hazard curve for three spectral periods for LA Bulk Mail site.

reflect seven hazard levels ranging from 50% in 5 years to 2% in 50 years for the site located in Northern California. The response spectra of the individual record along with seven hazard levels is shown in Fig. 6a. Further, the selected ground motions were far-field ground motions with pertinent properties, include peak ground acceleration (>0.2g) magnitude (>6.5), distance from source to site (10 km) and site class (D).

It should be noted that the ground motions records did not account for the characteristics of spectral shape (ε) of the rare ground motions that are likely to cause a collapse of the structures. It has been observed that ignoring the effect of spectral shape (ε) may under predict the median collapse capacity by 50%, on average [23,34]. The uncertainty in the collapse was accounted for by adjusting the fragility curve based on the method developed by Haselton et al. [23] where the expected epsilon, ε, value of 1.5 was used for the considered site and hazard level.

Fig. 6b shows the hazard curve of the site of interest, which describes the annual probability of exceedance of a ground motion intensity. The hazard curves for three different natural periods were obtained based on the seven hazard levels (Fig. 6a). The hazard curve permits the calculation of the mean annual frequency of collapse (λ_{col}) by integrating with the fragility curve.

7. Seismic performance results and discussions

7.1. Numerical results

The analysis results for the 18 archetype frame structures are summarized in Table 3 and Fig. 11 for the selected site in Los Angeles. It is worth noting that collapse predictions were based on the controlling component of the record pair and also accounted for uncertainties in spectral shape (ϵ) and modeling ($\sigma_{ln,modeling}$) as described in Section 3. The metric used for quantifying the seismic performance of each frame is tabulated in Table 3 including adjusted median collapse ($\hat{S}_{ct}$) obtained directly from the fragility curve (Fig. 2c), adjusted collapse margin ratio (ACMR) which is the ratio of adjusted median collapse capacity ($\hat{S}_{ct}$) and spectral acceleration $Sa_{MCER}(T_1)$ that has 2% probability of exceedance in 50 years motion, probability of collapse corresponding to spectral acceleration at the MCER level ($P[2/50]$), and mean annual frequency of

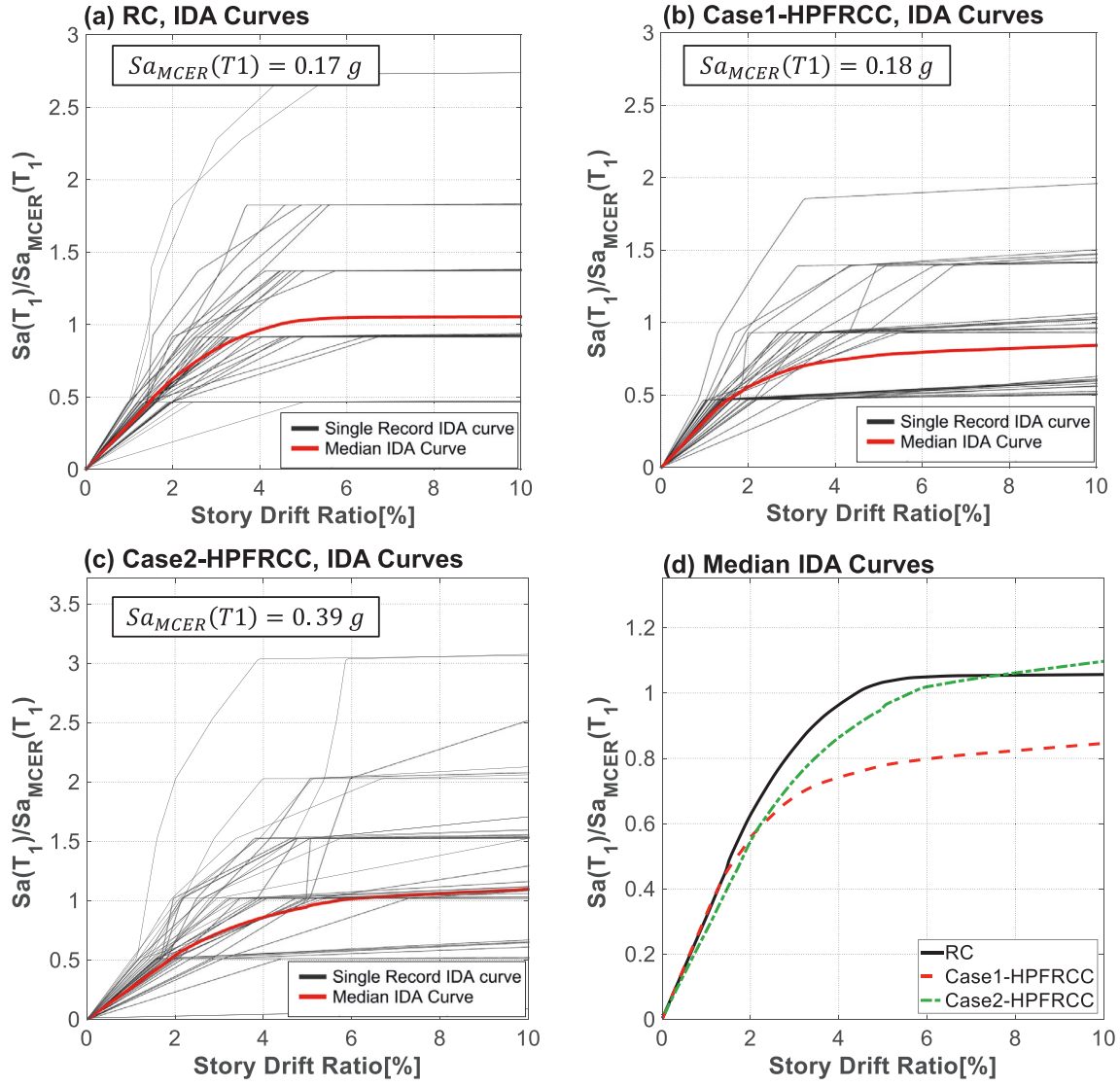

Fig. 7. Comparison of normalized IDA curves for twelve-story space frame building ID: 1014.

collapse (λ_{col}). The results published by Haselton et al. [23] are also tabulated in Table 3 for the RC frame referred to as 'RC-Haselton' for reference.

As shown in Table 3, the adjusted collapse margin ratios vary from 1.7 to 3.4, 1.4 to 2.9, and 1.98 to 3.5 for the RC, Case1-HPFRCC, and Case2-HPFRCC frame models with an average value of 2.25, 1.95 and 2.47 respectively. The probabilities of collapse ($P[2/50]$) conditioned on the 2% in 50 years ground motion range from 0.03 to 0.21, 0.05 to 0.29, 0.02 to 0.14 for the RC, Case1-HPFRCC, and Case2-HPFRCC frame models with an average value of 0.13, 0.18 and 0.09. Similarly, the mean annual frequency (λ_{col}) of collapse varies from 1.1 $\times 10^{-4}$ to 6.8 $\times 10^{-4}$, 1.6 $\times 10^{-4}$ to 12 $\times 10^{-4}$, 0.87 $\times 10^{-4}$ to 7.1 $\times 10^{-4}$ collapses/year for the RC, Case1-HPFRCC, and Case2-HPFRCC frame models with an average rate of 4.1, 6.8 and 3.9. The mean annual frequency further corresponds to the mean collapse return period of 2500, 1470, and 2570 years for three frame models, respectively.

Fig. 7 presents sample results from the incremental dynamic analysis for a twelve-story space-frame building (ID: 1014). The results are normalized by spectral acceleration, $Sa_{MCER}(T_1)$ at the MCER level for each archetype frame model for the purpose of comparison. Figs. 7a-c show the individual IDA curves and median curve for three corresponding frames represented by gray and red lines. The median IDA curves of three frame models are compared in Figs. 7d, where each IDA curve can be classified into three stages: (1) initial elastic stage at lower intensity levels, (2) inelastic stage with an increment of peak ground accelerations, and (3) a dynamically unstable phase where the slope of each curve became close to zero.

Case1-HPFRCC frame models showed a similar behavior as compared to the RC model until a spectral acceleration ratio of 0.5, at which point the response started to deviate significantly at a higher level of deformation demand. The predicted median collapse capacity ratio was 26% lower than the RC model. The reduction in the collapse capacity is attributed to the higher strength of the beams leading to a lower value of SCWB ratio (1.18) as compared to the RC model (1.7), on average, which restrained the hinge formation to the first story columns only and caused a soft story collapse mechanism.

Case 2-HPFRCC frame model showed higher deformation demand under the same level of spectral intensity ratio, as compared to the RC model, due to its higher natural period (T_1). However, the collapse margin ratio increased by a factor of 1.02 and 1.4 compared to the RC and Case1-HPFRCC frame models. The difference appeared to be due to the higher rotational capacity of reinforced HPFRCC beams. Further, design decisions that maintained the same strong column-weak beam relation (SCWB=1.7) as compared to the RC frame model aided in spreading

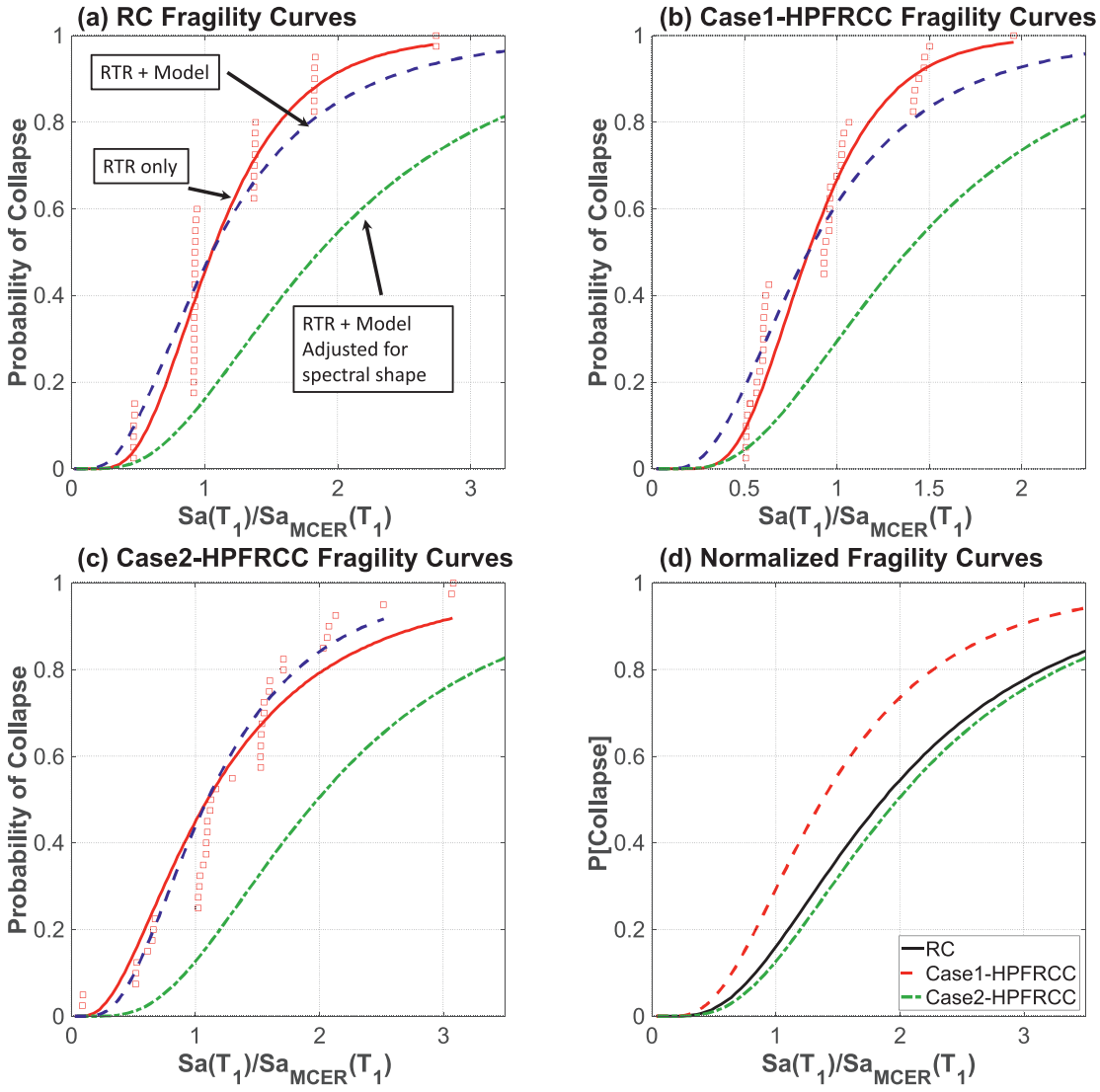

Fig. 8. Comparison of normalized IDA curves for twelve-story space frame building ID: 1014.

the hinge mechanism along the height of the frame and improved the energy dissipation of the structure.

The corresponding normalized fragility curves are shown in Figs. 8a-c for each frame model. Each figure illustrates the empirical collapse capacity, log-normally fitted collapse curve with respect to record-to-record variability ($\sigma_{ln,RTR}$), modeling uncertainty ($\sigma_{ln,modeling}$), and spectral shape (ϵ). The adjusted fragility curve for each frame model is further compared in Fig. 8d. The Case2-HPFRCC frame model showed the highest collapse safety of the three frame configurations considered. Compared to the RC frame model, the Case2-HPFRCC frame models have slightly higher collapse margin ratios, approximately 1.06 times larger, indicating a lower risk of collapse. The Case1-HPFRCC frame model suffered a strength discontinuity in the upper stories due to the higher strength of the beam, which decreased the collapse safety. Similarly, the probability of collapse ($P[2/50]$) from a 2% in a 50-year earthquake is also compared across the three frame configurations where the Case2-HPFRCC frame showed the lowest probability (0.13) followed by the RC frame (0.15) and the Case1-HPFRCC frame model (0.29).

The damage patterns of three frames are compared along the height of the frame for a representative ground motion under the same peak ground acceleration (PGA) value (3.0g) (Fig. 9). The damage accumulation is quantified as a rotation demand of each spring-hinge where the demand exceeds yielding (θ_y), 75% of capping ($0.75\theta_c$), capping (θ_c) and residual rotation (θ_r) are represented by cyan, green, orange and red colors, respectively. The corresponding damage against each limit state is classified as minor, moderate, significant, and collapse. The definition of performance levels coincides with limit states defined in ASCE 41-17 [49] for RC frame structures. The Case1-HPFRCC frame showed a soft-story mechanism due to the lower SCWB ratio, which led to an early yielding of columns, confining the inelastic deformation to the first story as illustrated in Fig. 9b. In contrast, the Case2-HPFRCC frame model showed multistory damage distribution similar to the RC frame model (Fig. 9c).

The distributions of story drift ratios along the height of the frames were also analyzed under the same ground motion. Fig. 10 shows the maximum story drift ratios of each frame model corresponding to the same earthquake intensity (PGA=3g). It is again observed that deformation in the upper stories of the Case1-HPFRCC frame model was lower than in the RC and Case2-HPFRCC frame models due to the soft story mechanism in the eleventh and first story. A maximum drift of 6.3% was observed at the first story right before the collapse as compared to a drift ratio of 4% and 3.6% for RC and Case2-HPFRCC frame models, respectively. For Case 2-HPFRCC frame models, no evidence of a soft story was observed. The largest drift observed at the first story of Case2-HPFRCC was 9% less than the RC frame. This difference is attributed to the higher natural period of the Case2-HPFRCC frame, which resulted

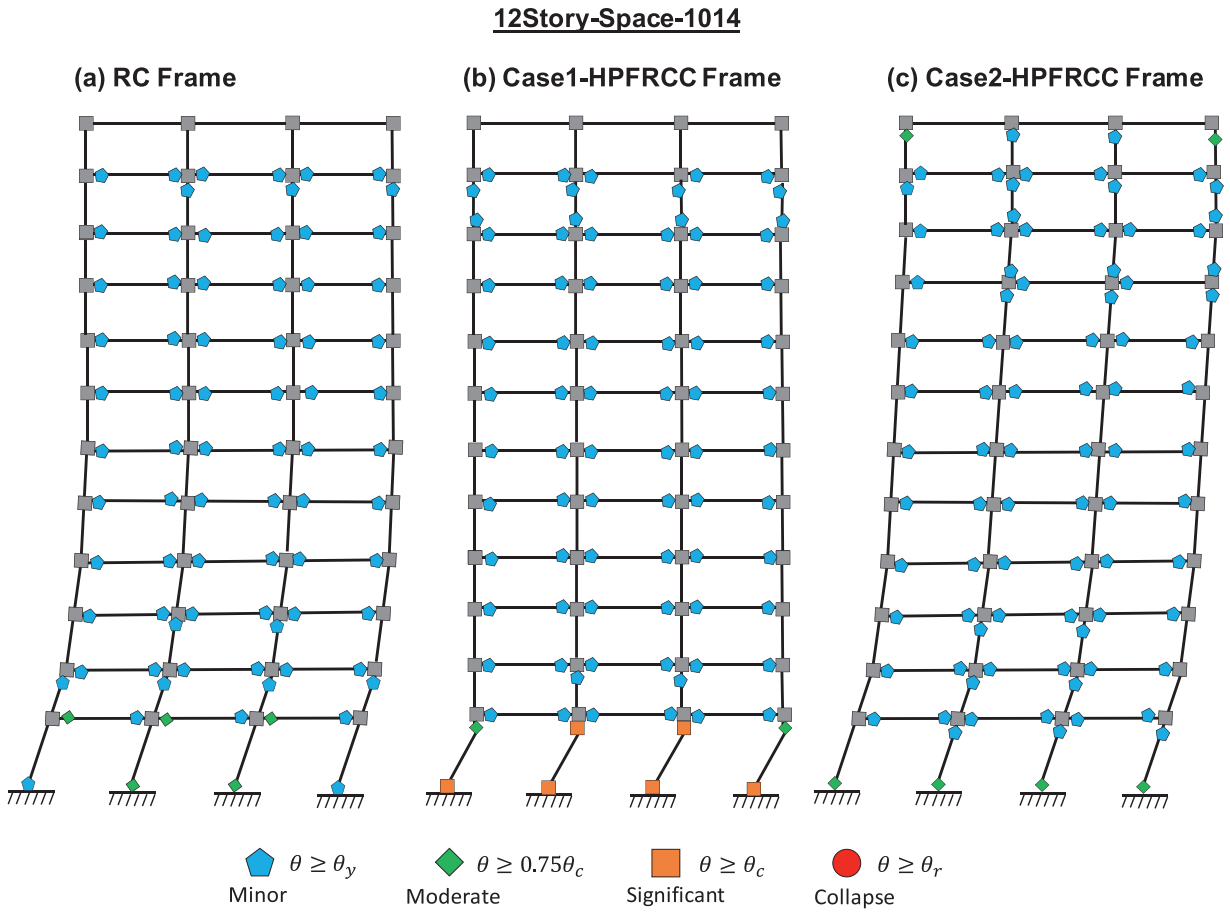

Fig. 9. Comparison of damage propagation for twelve-story space frame building ID: 1014 under earthquake record Northridge, 120,151 (PGA=3.0g).

in a reduction in the force and displacement demand according to the response spectra (Fig. 6a).

7.2. Effect of number of stories and frame configuration

The collapse performance of all archetype frames is compared across building heights and is differentiated with respect to perimeter and space frame configurations in Fig. 11. The relationship between ACMR and building height is illustrated in Fig. 11a. The results suggest that the collapse margin ratio decreases with an increased number of stories. This is attributed to the reduction in the rotational capacity of columns due to higher axial loads and predominant P-△ effects, which reduce the drift capacity of the structure due to negative stiffness. Further, the space frame buildings showed improved performance with ACMRs that were 26%, 23%, and 14% higher, on average, as compared to perimeter frame buildings for RC, Case1-HPFRCC, and Case2-HPFRCC models, respectively. This difference is due to the smaller P-△ effect, which increased the higher system ductility and strength. The results are in agreement with the existing finding for ductile and non-ductile RC frames [50,51]. Moreover, the ACMR for the Case2-HPFRCC frame was 9.7% and 26% greater than the RC and Case1-HPFRCC frames, on average. Regardless of height, the Case1-HPFRCC frame buildings showed the worst performance due to a soft-story mechanism, whereas the Case2-HPFRCC frame showed uniform distribution of damage along the height of the building (Fig. 9 and Fig. 10)

Fig. 11 b shows trends in the probability of collapse ($P[2/50]$) from a 2% in 50-year earthquake. Results showed similar trends where taller buildings have a higher probability of collapse. The trend was the same for perimeter frame buildings with collapse risks 60%, 40%, and 38% greater than the space frame buildings for RC, Case1-HPFRCC, and Case2-HPFRCC frame models. Further, the Case2-HPFRCC frames showed a reduced probability of collapse when compared to RC frames. The performance was better for perimeter frames (30% reduction in the probability of collapse) as compared to space frames (20% reduction).

The mean annual frequency of collapse (λ_{col}) is further compared in Fig. 11c for the site considered. Results illustrate a higher collapse risk with a larger number of stories, except the 12-story perimeter RC frame, which showed lower collapse risk due to a smaller value of log-normal standard deviation ($\sigma_{ln,Total}$=0.63) as compared to the 8-story perimeter RC frame ($\sigma_{ln,Total}$=0.65). Consequently, space frame buildings had lower annual rates of collapse with mean annual frequencies that were 1.5, 1.34, and 1.28 times lower than perimeter frame buildings for RC, Case1-HPFRCC, and Case2-HPFRCC frames. Further, the Case1-HPFRCC and RC frames are approximately 1.75 and 1.1 times more likely to collapse when compared to the Case2-HPFRCC frame, respectively. The difference in the estimated risk for RC and Case2-HPFRCC frames is more pronounced for space frames (1.14) as compared to the perimeter frames. Additionally, the mean annual frequency of collapse (λ_{col}) for a 12-story Case2-HPFRCC frame was higher than the RC frame model by 24%, on average. This could be attributed to the higher flexibility due to the reduction of beams in the Case2-HPFRCC frame leading to higher P-delta effects. This issue could be addressed by designing the structure with a response modification factor (R) calibrated to the dynamic characteristics of reinforced HPFRCC moment frames. However, due to the lack of research on the response modification factors, HPFRCC frame models were analyzed with a design that was based on the same value of the response modification factor.

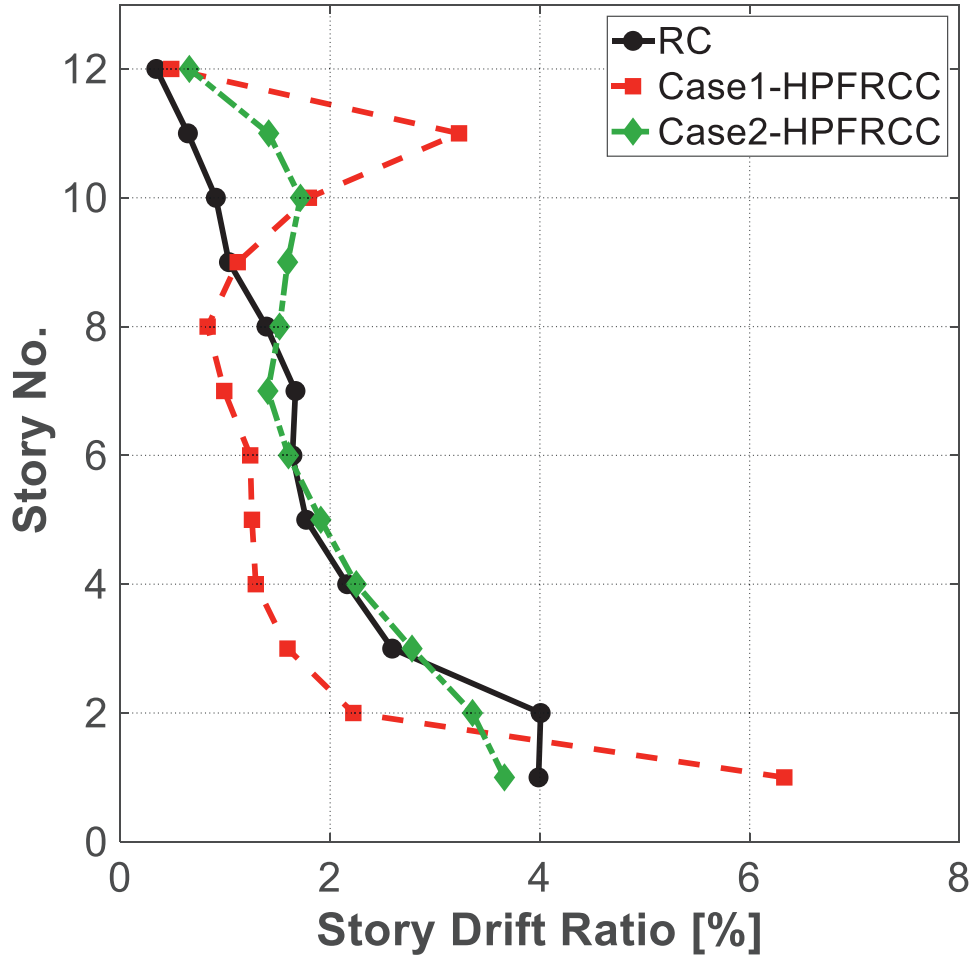

Fig. 10. Comparison of story drift ratio for twelve-story space frame building ID: 1014 under earthquake record Northridge, 120,151 (PGA=3.0g).

Finally, the collapse risk of Case2-HPFRCC frames was further compared with acceptable limits specified in FEMA P-695 [52]. The reported results show acceptable performance where the probability of collapse conditioned on the maximum considered earthquake intensity is ≤10% on average and less than 20% for each archetype model.

7.3. Concrete volume and steel weight

In addition to evaluating and comparing the probabilistic seismic performance, the concrete volume and reinforcing bar weight reduction are also compared for RC and Case2-HPFRCC frame models in Fig. 12 to demonstrate other potential benefits of HPFRCCs on construction. The concrete volume for Case2-HPFRCC frame models was reduced by a factor of 1.12, on average, and the volume reduction was two times higher for perimeter frames as compared to space frame buildings (Fig. 12a). This can be attributed to the reduction of the beam cross-section height (h) along the height of the building as compared to space frames, where cross-section sizes were reduced until a particular story. The reinforcement ratio was reduced for the remaining stories to achieve a similar strength for reinforced HPFRCC beams as compared to RC beams.

Fig. 12 b shows the reduction in reinforcing bar weight for Case2-HPFRCC frames as compared to RC frames for perimeter and space frame configurations. The reinforcing bar weight in beams of Case2-HPFRCC frames was reduced by 11%, on average. The area of steel was decreased despite increasing the reinforcement ratio in the beams for Case2-HPFRCC frame models because of a smaller cross-section height (h). These results imply significant potential benefits from a construction standpoint while maintaining (or improving) seismic system-level response. More research in this area including studies on the life-cycle costs of HPFRCC systems and the cost of fibers in ductile concrete system will provide more well-understood potential financial incentives for the use of high-performance materials in seismic applications.

8. Conclusion

This study presents the seismic performance of 18 RC frame models with heights ranging from four to twelve stories and two framing systems: perimeter and space frames. In addition to conventional RC frames designed by Haselton et al. [23], two design variants were considered in which concrete was replaced by a representative HPFRCC material in the plastic-hinge region of the beams. In the first variant (Case1-HPFRCC), the reinforced HPFRCC beam hinge properties were selected to mirror the section details designed by Haselton et al. [23] such that only the material (HPFRCC vs. concrete) was replaced and all other section properties were the same. Alternatively, the second variant (Case2-HPFRCC) used reduced beam sections to account for the higher flexural and shear strength of the reinforced HPFRCC to achieve the same SCWB as the conventional RC frames. The numerical modeling approach adopted for conventional RC frames was based on recommendations provided by Haselton et al. [23], and a modeling framework adopted for reinforced HPFRCC hinges was based on the method developed by Tariq et al. [22]. Numerical models were subjected to incremental dynamic analysis (IDA) for the evaluation of seismic performance.

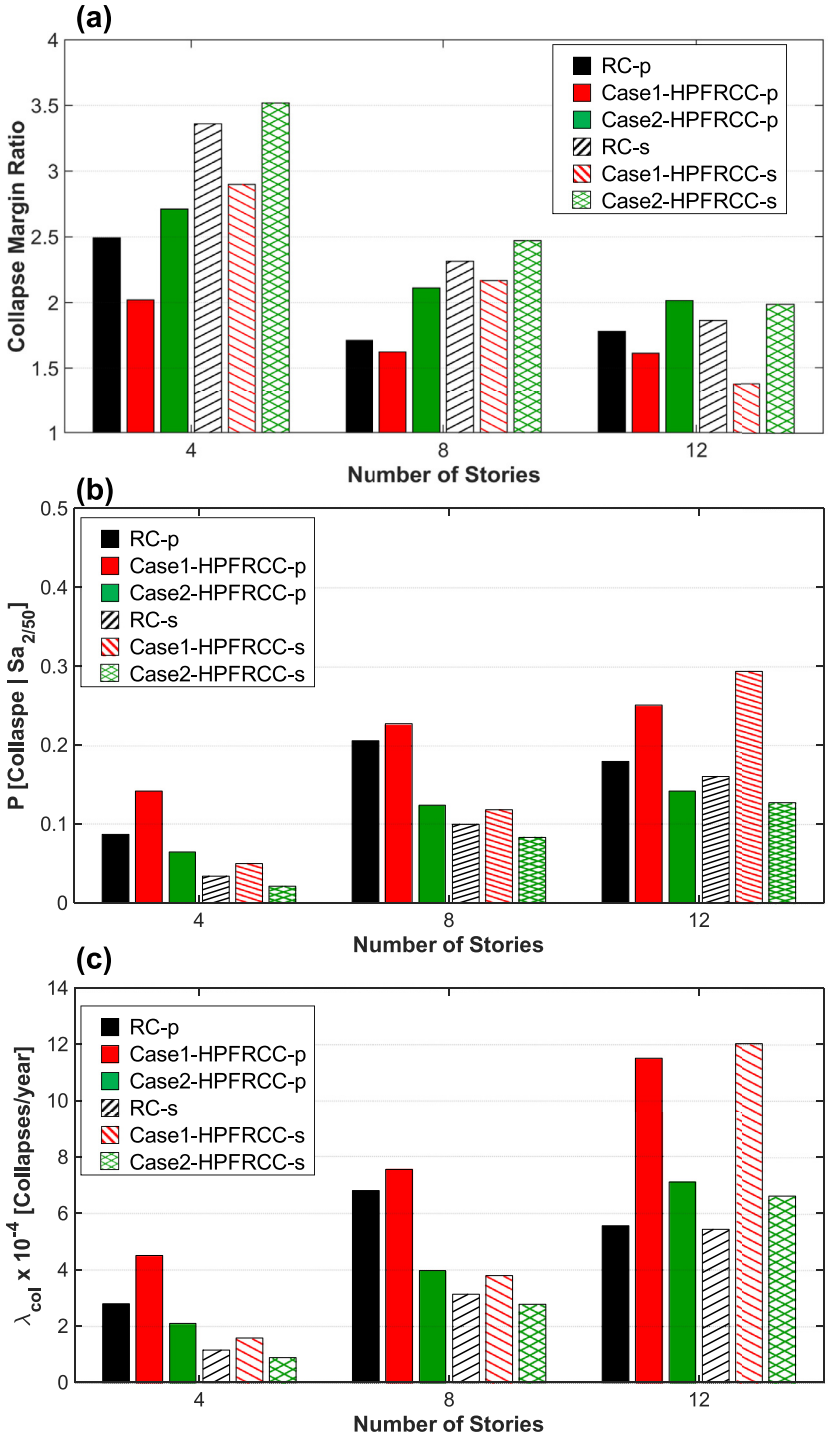

Fig. 11. Comparison of collapse risk assessment as a function of the number of stories (a) collapse margin ratio (b) Probability of collapse at 2% in 50 years motion (c) mean annual frequency of collapse.

The eigenvalue results showed a reduction in the initial stiffness of HPFRCC frames due to a lower modulus of elasticity, resulting in a higher fundamental period. The Case2-HPFRCC frame had the highest flexibility due to beam height reduction and lower material stiffness. Findings from probabilistic collapse assessment suggest similar performance between the Case1-HPFRCC frame and the RC frame at lower intensity levels. A soft-story mechanism governed ultimate failure in the Case1-HPFRCC frame due to the lower SCWB ratio caused by the high strength of reinforced HPFRCC beams. The Case2-HPFRCC frame model illustrated higher deformation at lower intensities of ground shaking; however, performance at collapse demonstrated better performance compared to RC and Case1-HPFRCC frame models. A distributed plastic-hinge mechanism was observed along the height of the building. One can achieve seismic performance that is similar to a code-conforming reinforced concrete frame by redesigning beam-cross sections with reinforced HPFRCC beams while using less material.

This assessment found that collapse risk increased with structure height, and perimeter frame systems were more vulnerable than space

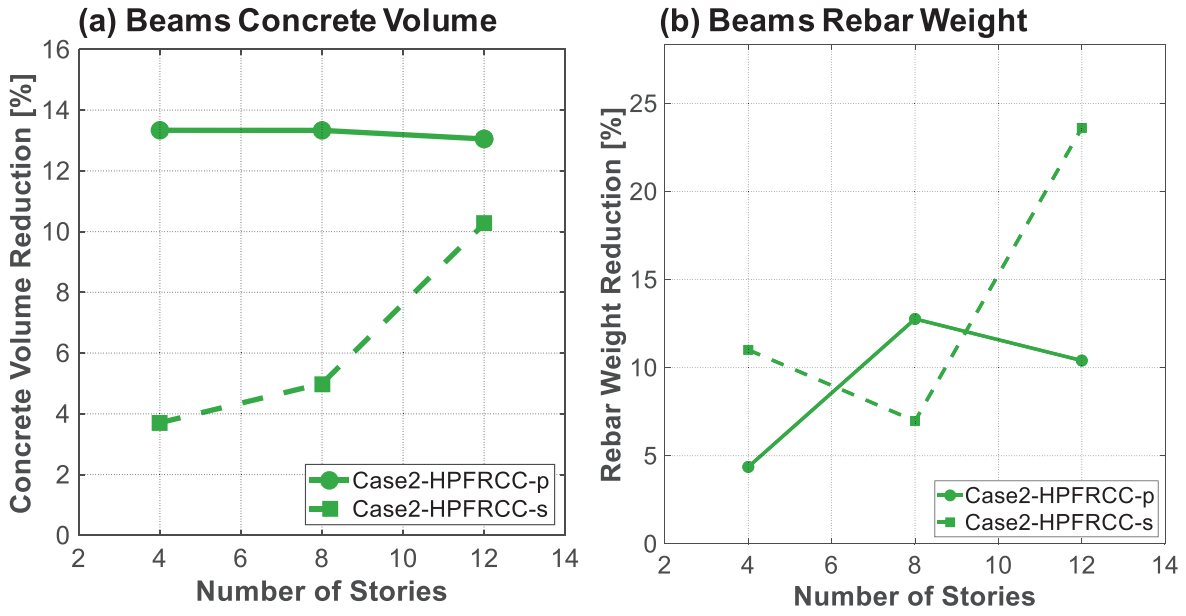

Fig. 12. Comparison of concrete volume and reinforcing bar weight reduction in case2-HPFRCC frame model with respect to RC frame model.

frame buildings due to predominant P-△ effects. Comparing the response of Case1-HPFRCC frames with RC frames showed that the margin against collapse (ACMR) reduced by 13% and the probability of collapse ($P[2/50]$) increased by 38%. This increase also corresponded to a 64% higher mean annual frequency of collapse (λ_{col}). The reduced performance was due to a lower strong column-weak beam (SCWB) ratio, which caused localized damage in one story. Case1-HPFRCC frames were considered in this analysis to quantify the collapse risk and disseminate the performance among the practicing engineering community. When frames are designed using existing approaches for RC structures by simply replacing the concrete with HPFRCC materials, there can be unintended consequences.

In contrast, Case 2-HPFRCC frames showed an increase in seismic performance, where the margin against collapse (ACMR) increased by 9%. The probability of collapse ($P[2/50]$) and mean annual frequency of collapse (λ_{col}) were reduced by 20% and 26%, on average, as compared to RC frame models. The increase in the collapse safety is due to the design decisions to maintain a consistent SCWB ratio and the deformation capacity of HPFRCC members, which helped spread damage along the height of the building, increased the system level energy dissipation capacity.

In addition to analyzing collapse safety, a comparison for material use was also made. The Case2-HPFRCC frames resulted in a concrete volume reduction of approximately 10%, on average, as compared to RC structures. This shows that seismic performance can be maintained while reducing material consumption when using advanced materials.

The dynamic analysis in this study included a variety of approximations such as scaling the ground motions to simulate the intense earthquake with a lower probability of occurrence, selection of a simplified two-dimensional model, and developing numerical models that are limited to certain variables and unable to capture the axial-flexure interaction. The large uncertainty in record-to-record variability and modeling uncertainty affected collapse predictions significantly. However, the results showed relative collapse behavior and can be used for improving design approaches for buildings employing fiber-reinforced cementitious composite materials. Further, the quantitative risk assessment presented here offers new knowledge on how practicing engineers must be aware of the effects of material replacement. Results also encourage researchers to conduct more experimental testing to validate the numerical models used in this study.

The seismic performance of systems can be improved by completely replacing the concrete with HPFRCC in beam and column plastic-hinge regions. This would require developing design parameters, improving numerical models, and enhancing probabilistic collapse predictions. The accuracy of collapse safety is based on the accuracy of numerical models whose reliability hinges upon an extensive experimental database. Hence, a number of recommendations are proposed to improve the design procedure of HPFRCC frames.

To begin, the upper and lower limit on reinforcement ratios or strain limits should be developed to identify the various failure modes in reinforced HPFRCC, such as crushing, fracture, and bar buckling. These limits will dictate the design of reinforcement in reinforced HPFRCC beams. Recent research by Shao et al. [16] has begun to propose lower-bound reinforcement limits, which should be investigated further in the context of seismic detailing and modeling.

Next, this study examined the use of HPFRCCs in beam regions due to the lack of data available to develop modeling approaches for column elements. Experimental testing should be conducted on reinforced HPFRCC specimens with varying axial loads and shear span-to-depth ratios. Corresponding limits on axial loads and shear spans should be identified, and improvements to the plastic hinge length and rotational capacity of these elements should be determined. Relevant experimental testing and accompanying numerical models on the effects of axial load across a range of HPFRCC materials are underway by the last author and will add to the understanding of how these materials can improve the response of seismic systems.

Collapse performance can also be evaluated by varying the design in terms of SCWB ratios, design base-shear strength and design story drift ratios. This could help code committees to codify design provisions better. Furthermore, the accuracy in performing the nonlinear dynamic analysis to estimate the fragility curve can be improved by selecting different intensity levels, each of which has its own ground motion record [53,54]. Finally, the collapse assessment can also be extended by utilizing near-field ground motions and would be useful to consider other site locations and investigate their impact on the annual rate of collapse.

Declaration of competing interest

The authors declare the following financial interests/personal relationships which may be considered as potential competing interests:

Matthew J. Bandelt reports financial support was provided by National Science Foundation. Matthew J. Bandelt reports a relationship with National Science Foundation that includes: funding grants.

Acknowledgments

This material is based upon work supported by the National Science Foundation under Grant No. 2141955. Any opinions, findings, conclusions, or recommendations expressed in this material are those of the author(s) and do not necessarily reflect the views of the National Science Foundation. The authors also gratefully acknowledge support from the John A. Reif, Jr. Department of Civil and Environmental Engineering at New Jersey Institute of Technology.

Appendix A. Supplementary Details on the Geometry of the Selected Archtype Frames

The Appendix A presents the schematic of cross-sectional details for each frame type. The cross-section of beams include cross-section width (b), height (h), top reinforcement ratio (ρ_t) and bottom reinforcement ratio ρ_b for all the archetype frames considered as shown in Figs. A.13, A.14, A.15, A.16, A.17, A.18. The Beam cross-section details for Case1-HPFRCC frames are identical to RC frames, whereas sectional details have been designed to maintain a similar strong column-weak beam (SCWB) relation compared to the RC in Case2-HPFRCC frames. The sectional geometry of columns is also illustrated at the bottom of the RC frame for all the buildings. The column's sizes are uniform along the height of the building.

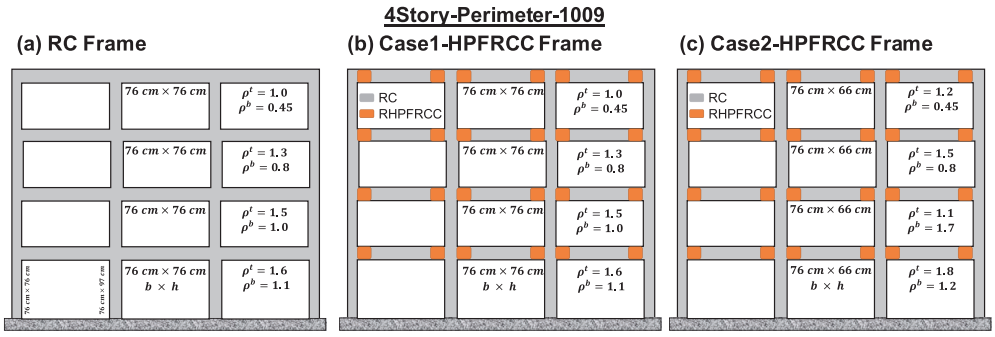

Fig. A.13. Summary of beam sectional details for four-story perimeter frame building, ID:1009.

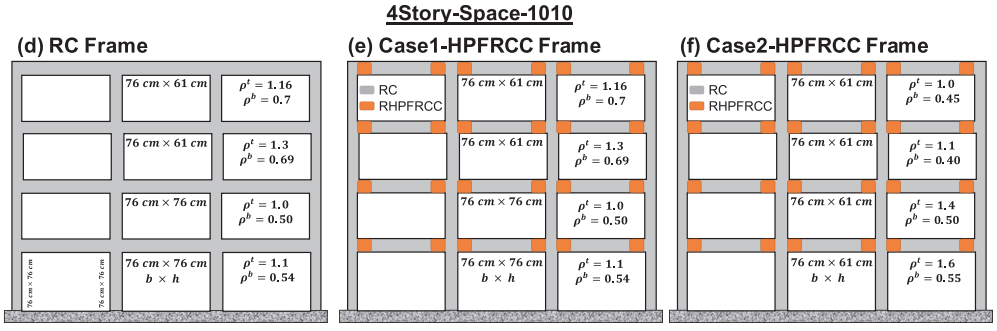

Fig. A.14. Summary of beam sectional details for four-story space frame building, ID:1010.

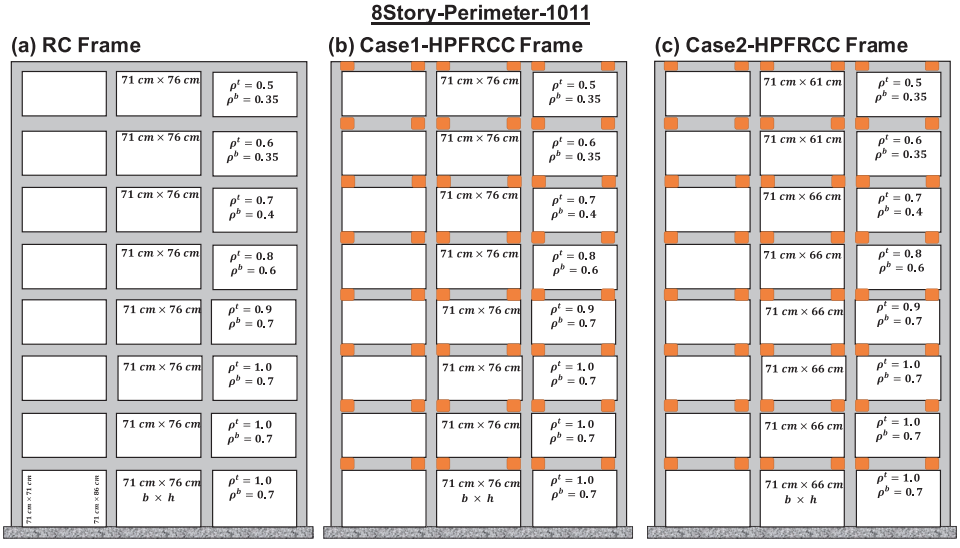

Fig. A.15. Summary of sectional details for eight-story perimeter frame building, ID:1011.

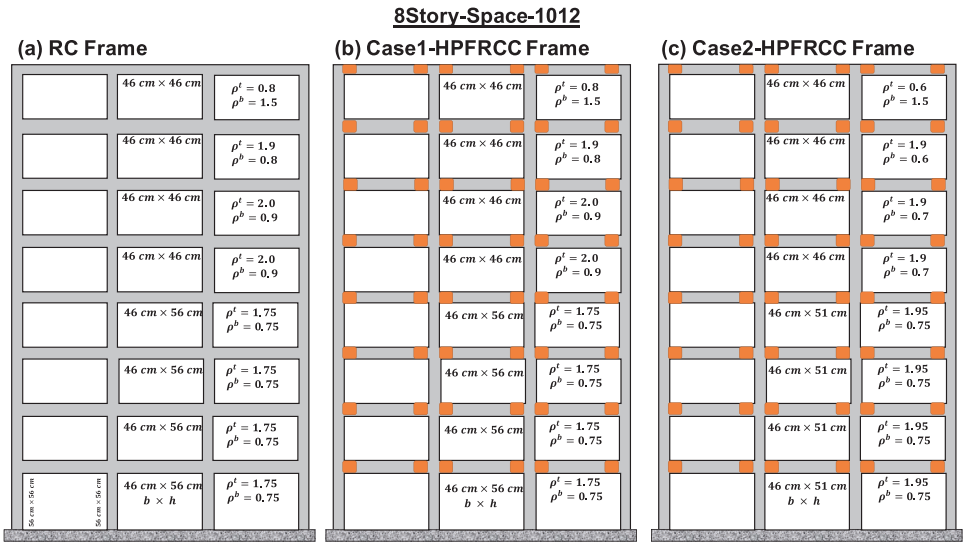

Fig. A.16. Summary of beam sectional details for eight-story space frame building, ID:1012.

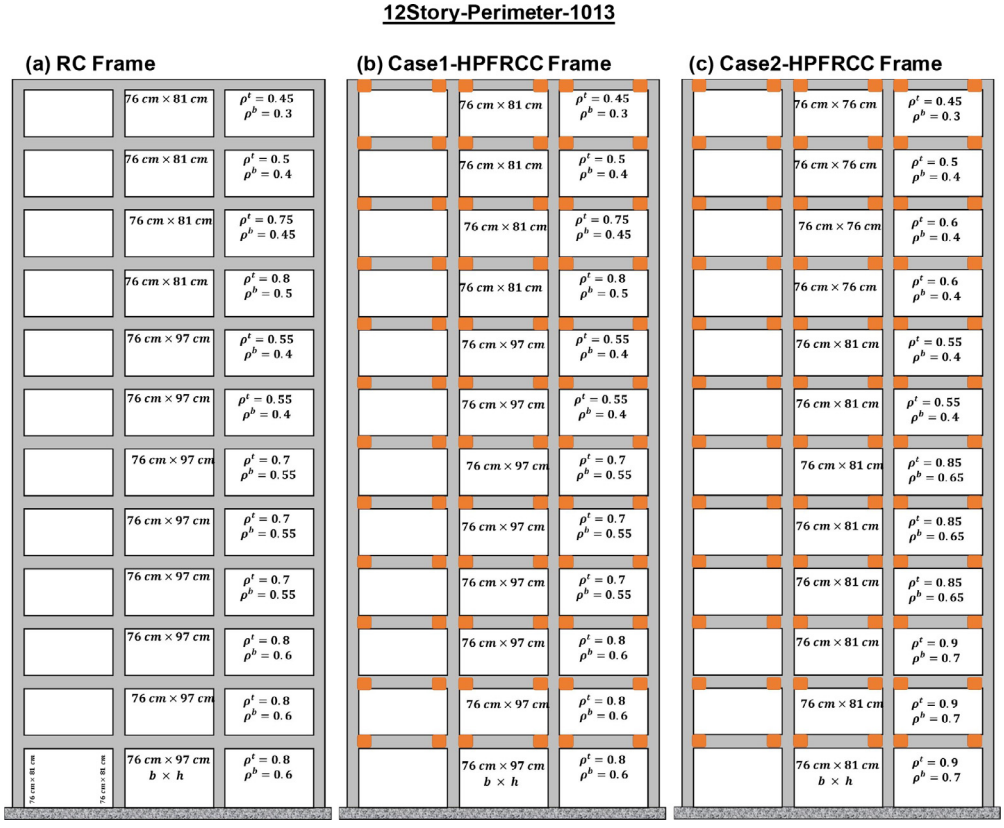

Fig. A.17. Summary of beam sectional details for twelve-story perimeter frame building, ID:1013.

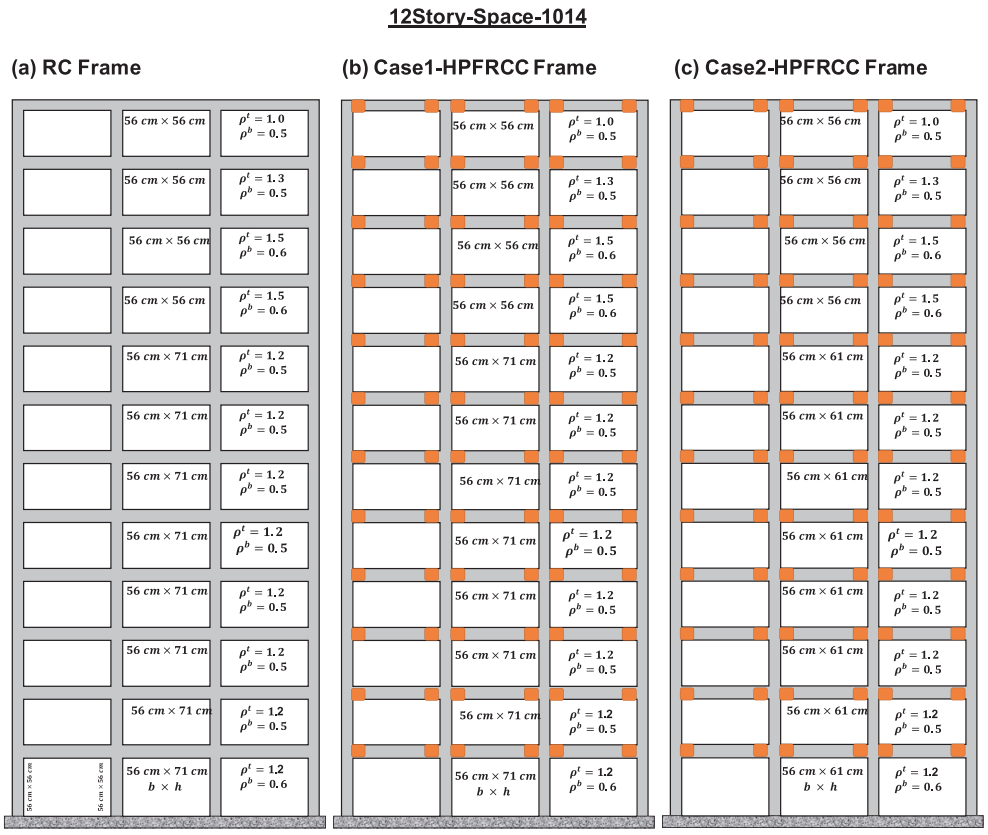

Fig. A.18. Summary of beam sectional details for twelve-story space frame building, ID:1014.

References

[1] Moehle JP, Hooper JD, Lubke CD. Seismic design of reinforced concrete special moment frames: a guide for practing engineers. US Department of Commerce, Technology Administration, National Institute of ; 2008.

[2] ACI. 318-19 building code requirements for structuralconcreteand commentary. American Concrete Institute; 2019. doi:1014359/51716937.

[3] Aoude H, Hosinieh MM, Cook WD, Mitchell D. Behavior of rectangular columns constructed with SCC and steel fibers. J Struct Eng 2015;141(8):04014191.

[4] Jen G, Trono W, Ostertag CP. Self-consolidating hybrid fiber reinforced concrete: development, properties and composite behavior. Constr Build Mater 2016;104:63–71.

[5] Li VC, Wang S. Microstructure variability and macroscopic composite properties of high performance fiber reinforced cementitious composites. Probab Eng Mech 2006;21(3):201–6.

[6] Naaman AE, Reinhardt HW. Setting the stage, toward performance based classification of FRC composites. In: High Performance Fiber Reinforced Cement Composites (HPFRCC 4), Proc. of the 4th Int. RILEM Workshop; 2003.

[7] Fischer G, Li VC. Effect of matrix ductility on the performance of reinforced ECC column members under reversed cyclic loading conditions. ACI Struct J 2002(99):269–78. doi:10.14359/12343.

[8] Parra-Montesinos GJ, Chompreda P. Deformation capacity and shear strength of fiber-reinforced cement composite flexural members subjected to displacement reversals. J Struct Eng 2007;133(3):421–31. doi:10.1061/(asce)0733-9445(2007)133:3(421).

[9] Yuan F, Pan J, Xu Z, Leung CKY. A comparison of engineered cementitious composites versus normal concrete in beam-column joints under reversed cyclic loading. Mater Struct 2013;46(1–2):145–59. doi:10.1617/s11527-012-9890-6.

[10] Canbolat BA, Parra-montesinos GJ, Wight JK. Experimental study on seismic behavior of high-performance fiber-reinforced cement composite coupling beams. ACI Struct J 2005(102):159–66. doi:10.14359/13541.

[11] Dang Z, Liang X, Deng M. Cyclic behavior of shear walls with HPFRCCs in the inelastic deformation critical region. Struct Des Tall Special Build 2016;25(17):886–903. doi:10.1002/tal.1288.

[12] Wu C, Pan Z, Su RKL, Leung CKY, Meng S. Seismic behavior of steel reinforced ECC columns under constant axial loading and reversed cyclic lateral loading. Mater Struct/Materiaux et Construct 2017;50(1):1–15. doi:10.1617/s11527-016-0947-9.

[13] Xu L, Pan J, Chen J. Mechanical behavior of ECC and ECC/RC composite columns under reversed cyclic loading. J Mater Civ Eng 2017;29(9):04017097. doi:10.1061/(asce)mt.1943-5533.0001950.

[14] Bandelt MJ, Billington SL. Impact of reinforcement ratio and loading type on the deformation capacity of high-performance fiber-reinforced cementitious composites reinforced with mild steel. J Struct Eng 2016;142(10):457–63. doi:10.1061/(ASCE)ST.1943-541X.0001562.

[15] Frank TE, Lepech MD, Billington SL. Experimental testing of reinforced concrete and reinforced ECC flexural members subjected to various cyclic deformation histories. Mater Struct 2017;50(5):232. doi:10.1617/s11527-017-1102-y.

[16] Shao Y, Billington SL. Predicting the two predominant flexural failure paths of longitudinally reinforced high-performance fiber-reinforced cementitious composite structural members. Eng Struct 2019;199:109581.

[17] Bandelt MJ, Billington SL. Simulation of deformation capacity in reinforced high-performance fiber-reinforced cementitious composite flexural members. J Struct Eng 2018(April). doi:10.1061/(ASCE)ST.1943-541X.0002174.

[18] Pokhrel M, Bandelt MJ. Material properties and structural characteristics influencing deformation capacity and plasticity in reinforced ductile cement-based composite structural components. Compos Struct 2019;217:81–90. doi:10.1016/j.cageo.2011.03.003.As.

[19] Pokhrel M, Bandelt MJ. Plastic hinge behavior and rotation capacity in reinforced ductile concrete flexural members. Eng Struct 2019;200(May):109699. doi:10.1016/j.engstruct.2019.109699.

[20] Tariq H, Jampole EA, Bandelt MJ. Fiber-hinge modeling of engineered cementitious composite flexural members under large deformations. Eng Struct 2019;182:62–78. doi:10.1016/j.engstruct.2018.11.076.

[21] Kheyroddin A, Naderpour H. Plastic hinge rotation capacity of reinforced concrete beams. Int J Civil Eng 2007;5(1):30–47. doi:10.1061/(ASCE)ST.1943-541X.0000858. http://ijce.iust.ac.ir/browse.php?a_code=A-10-451-6&slc_lang=en&sid=1

[22] Tariq H, Jampole EA, Bandelt MJ. Development and application of spring hinge models to simulate reinforced ductile concrete structural components under cyclic loading. J Struct Eng 2021;147(2):04020322.

[23] Haselton CB, Deierlein GG. Assessing seismic collapse safety of modern reinforced concrete moment frame buildings. The John A Blume Earthquake Engineering Center, Department of Civil and Environmental Engineering, Stanford University, Palo Alto, California 2007.

[24] Mirzahosseini H, Mirhosseini SM, Zeighami E. Robustness assessment of RC frame buildings with HPFRCC subjected to progressive collapse. Result Eng 2023;17:100809.

[25] Hemmati A, Kheyroddin A, Sharbatdar M, Park Y, Abolmaali A. Ductile behavior of high performance fiber reinforced cementitious composite (HPFRCC) frames. Constr Build Mater 2016;115:681–9.

[26] Nguyen W, Shao Y, Billington SL, Bandelt MJ, Ostertag CP. High-performance fiber-reinforced cementitious composites for seismic design: a review of columns. In: The 17th World Conference on Earthquake Engineering. Sendai: International Association for Earthquake Engineering; 2021.

[27] Ning N, Qu W, Ma ZJ. Design recommendations for achieving “strong column-weak beam” in RC frames. Eng Struct 2016;126:343–52.
[28] Cavaco E, Pacheco I, Camara J. Detailing of concrete-to-concrete interfaces for improved ductility. Eng Struct 2018;156:210–23.
[29] Paulay T. The design of ductile reinforced concrete structural walls for earthquake resistance. Earthquake Spectra 1986;2(4):783–823.
[30] Engineers ASoC. Minimum design loads and associated criteria for buildings and other structures. American Society of Civil Engineers; 2017.
[31] Moreno DM, Trono W, Jen G, Ostertag C, Billington SL. Tension stiffening in reinforced high performance fiber reinforced cement-based composites. Cem Concr Compos 2014;50:36–46. doi:10.1016/j.cemconcomp.2014.03.004.
[32] Frank TE. Response of reinforced engineered cementitious composite flexural members subjected to various cyclic deformation histories. Stanford University; 2017. Ph.D. thesis.
[33] Ibarra LF, Medina RA, Krawinkler H. Hysteretic models that incorporate strength and stiffness deterioration. Earthquake Eng Struct Dyn 2005;34(12):1489–511. doi:10.1002/eqe.495.
[34] Zareian F, Krawinkler H. Assessment of probability of collapse and design for collapse safety. Earthquake Eng Struct Dyn 2007(056):1–6. doi:10.1002/eqe.
[35] Vamvatsikos D, Allin Cornell C. Incremental dynamic analysis. Earthquake Eng Struct Dyn 2002;31(3):491–514. doi:10.1002/eqe.141.
[36] Baker JW. Efficient analytical fragility function fitting using dynamic structural analysis. Earthquake Spectra 2015;31(1):579–99. doi:10.1193/021113EQS025M.
[37] Haselton CB, Baker JW, Liel AB, Deierlein GG. Accounting for ground-motion spectral shape characteristics in structural collapse assessment through an adjustment for epsilon. J Struct Eng 2011;137(3):332–44. doi:10.1061/(ASCE)ST.1943-541X.0000103.
[38] (ACI) ACI. Building code requirements for structural concrete and commentary. aci 318-14. Farmington Hills, MI: ACI.; 2014.
[39] ASCE. Minimum design loads for buildings and other structures; 2002.
[40] McKenna F., Fenves G.L., Scott M.H., Jeremić B.. Open system for earthquake engineering simulationhttp://opensees.berkeley.edu. 2000.
[41] Ibarra LF, Medina RA, Krawinkler H. Hysteretic models that incorporate strength and stiffness deterioration. Earthquake Eng Struct Dyn 2005;34(12):1489–511. doi:10.1002/eqe.495.
[42] Lowes LN, Altoontash A. Modeling reinforced-concrete beam-column joints subjected to cyclic loading. J Struct Eng 2003;129(12):1686–97. doi:10.1061/(ASCE)0733-9445(2003)129:12(1686). http://ascelibrary.org/doi/10.1061/%28ASCE%290733-9445%282003%29129%3A12%281686%29
[43] Lowes LN, Mitra N, Altoontash A. A beam-column joint model for simulating the earthquake response of reinforced concrete frames. PEER Report 2003/10 2004.
[44] Lepech MD, Li VC. Large-scale processing of engineered cementitious composites. ACI Struct J 2008;31(10):744–53. doi:10.1016/j.cemconcomp.2009.07.002.
[45] Ellingwood B, T V Galam bos J, MacGregor G, Cornell CA. Development of a probability based load criterion for american national standard A58: building code requirements for minimum design loads in buildings and other structures. US Department of Commerce, National Bureau of Standards; 1980.
[46] Robertson I. Research progress presentation. In: Pacific Earthquake Engineering Research Center Annual Meeting, January 17–18, 2002, Oakland,; 2002. p. 886–903.
[47] Zareian F, Medina RA. A practical method for proper modeling of structural damping in inelastic plane structural systems. Comput Struct 2010;88(1–2):45–53. doi:10.1016/j.compstruc.2009.08.001.
[48] Goulet CA, Haselton CB, Mitrani-reiser J, Beck JL, Deierlein GG, Porter KA, Stewart JP. Evaluation of the seismic performance of a code-conforming reinforced-concrete frame building-from seismic hazard to collapse safety and economic losses. Earthquake Eng Struct Dyn 2007(056):1–6. doi:10.1002/eqe.
[49] ASCE -. Seismic evaluation and retrofit of existing buildings. American Society of Civil Engineers Reston, VA; 2017.
[50] Haselton CB, Liel AB, Deierlein GG, Dean BS, Chou JH. Seismic collapse safety of reinforced concrete buildings. i: assessment of ductile moment frames. J Struct Eng 2011;137(4):481–91. doi:10.1061/(ASCE)ST.1943-541X.0000318.
[51] Liel AB, Haselton CB, Deierlein GG. Seismic collapse safety of reinforced concrete buildings. II: comparative assessment of nonductile and ductile moment frames. J Struct Eng 2011;137(4):492–502. doi:10.1061/(ASCE)ST.1943-541X.0000275.
[52] (ATC) ATC. Quantification of building seismic performance factors. Tech. Rep.. Structural Research Series 465, Civil Engineering Studies, University of Illinois, Urbana, Illinois; 2009.
[53] Jalayer F. Direct probabilistic seismic analysis: implementing non-linear dynamic assessments. Stanford University; 2003.
[54] Baker JW. Trade-offs in ground motion selection techniques for collapse assessment of structures. In: Vienna Congress on Recent Advances in Earthquake Engineering and Structural Dynamics, vol. 2013; 2013. p. 28–30.